The consistency of the AFM measurements for four different materials strongly suggests that this phenomenon is universal for atomically thin sheets that are loosely adhered to a substrate or freely suspended. This reveals a new mechanism of enhanced friction for quasi-2D materials based on elastic compliance. Because the effect is suppressed when the sheet is attached to a strongly adhering substrate, the results indicate an avenue to controlling nanoscale friction for these materials. Therefore, these results can potentially aid in the rational design and use of materials for nanomechanical applications, including nanolubricants and components in micro- and nanoeletromechanical systems devices.

References and Notes

1. H. Park *et al.*, *Nature* **407**, 57 (2000).
2. A. I. Yanson, G. R. Bollinger, H. E. van den Brom, N. Agrait, J. M. van Ruitenbeek, *Nature* **395**, 783 (1998).
3. A. K. Geim, *Science* **324**, 1530 (2009).
4. K. S. Novoselov *et al.*, *Science* **306**, 666 (2004).
5. I. Meric *et al.*, *Nat. Nanotechnol.* **3**, 654 (2008).
6. K. S. Novoselov *et al.*, *Proc. Natl. Acad. Sci. U.S.A.* **102**, 10451 (2005).
7. C. Donnet, A. Erdemir, *Surf. Coat. Tech.* **180-181**, 76 (2004).
8. I. L. Singer, H. M. Pollock, *Fundamentals of Friction: Macroscopic and Microscopic Processes* (Kluwer, Dordrecht, Netherlands, 1992).
9. T. Filleter *et al.*, *Phys. Rev. Lett.* **102**, 86102 (2009).
10. M. Tortonese, M. Kirk, *Proc. Soc. Photo. Opt. Instrum. Eng.* **3009**, 53 (1997).
11. P. Nemes-Incze, Z. Osváth, K. Kamarás, L. P. Biró, *Carbon* **46**, 1435 (2008).
12. Sample preparation, additional measurement results, and finite element modeling are available as supporting material on *Science* Online.
13. A. C. Ferrari *et al.*, *Phys. Rev. Lett.* **97**, 187401 (2006).
14. I. Szlufarska, M. Chandross, R. W. Carpick, *J. Phys. D Appl. Phys.* **41**, 123001 (2008).
15. Q. Li, K. S. Kim, A. Rydberg, *Rev. Sci. Instrum.* **77**, 65105 (2006).
16. J. E. Sader, J. W. M. Chon, P. Mulvaney, *Rev. Sci. Instrum.* **70**, 3967 (1999).
17. K. L. Johnson, *Contact Mechanics* (Cambridge Univ. Press, Cambridge, 1985).
18. C. H. Lui, L. Liu, K. F. Mak, G. W. Flynn, T. F. Heinz, *Nature* **462**, 339 (2009).
19. C. M. Mate, G. M. McClelland, R. Erlandsson, S. Chiang, *Phys. Rev. Lett.* **59**, 1942 (1987).
20. S. N. Medyanik, W. K. Liu, I.-H. Sung, R. W. Carpick, *Phys. Rev. Lett.* **97**, 136106 (2006).
21. X. Zhao, S. R. Phillpot, W. G. Sawyer, S. B. Sinnott, S. S. Perry, *Phys. Rev. Lett.* **102**, 186102 (2009).
22. J.-A. Ruan, B. Bhushan, *J. Appl. Phys.* **76**, 5022 (1994).
23. S. Fujisawa, E. Kishi, Y. Sugawara, S. Morita, *Phys. Rev. B* **51**, 7849 (1995).
24. K. Nakada, M. Fujita, G. Dresselhaus, M. S. Dresselhaus, *Phys. Rev. B* **54**, 17954 (1996).
25. M. Y. Han, B. Ozyilmaz, Y. Zhang, P. Kim, *Phys. Rev. Lett.* **98**, 206805 (2007).
26. M. Cieplak, E. D. Smith, M. O. Robbins, *Science* **265**, 1209 (1994).
27. B. N. J. Persson, A. I. Volokitin, *J. Chem. Phys.* **103**, 8679 (1995).
28. A. P. Merkle, L. D. Marks, *Tribol. Lett.* **26**, 73 (2007).
29. K. R. Shull, *Mater. Sci. Eng. Rep.* **36**, 1 (2002).
30. M. H. Müser, *Europhys. Lett.* **66**, 97 (2004).
31. L. Prandtl, *Z. Angew. Math. Mech.* **8**, 85 (1928).

32. We acknowledge support from the NSF under awards NSF/MRSEC (no. DMR-0520020) (R.W.C.), CMMI-0800154 (R.W.C.), CHE-0117752 (J.H.), and CMMI-0927891 (J.H.); the New York State Office of Science, Technology, and Academic Research (NYSTAR) (J.H.); the Defense Advanced Research Projects Agency (DARPA) Center on Nanoscale Science and Technology for Integrated Micro/Nano-Electromechanical Transducers (iMINT, grant HR0011-06-1-0048) (J.H.); Air Force Office of Scientific Research (AFOSR) (MURI FA955009-1-0705) (J.H.); and the Swiss NSF and its National Centers of Competence in Research (NCCR) MaNEP (H.B.). We thank Momentive Performance Materials, Advanced Diamond Technologies, and C. H. Lui for supplying h-BN powder, diamond-coated AFM probes, and graphene samples on mica, respectively. We acknowledge helpful discussions with J. Li, M. Müser, and L. Forró.

Supporting Online Material

www.sciencemag.org/cgi/content/full/328/5974/76/DC1
Materials and Methods
Figs. S1 to S8
References

3 November 2009; accepted 17 February 2010
10.1126/science.1184167

A Stratified Redox Model for the Ediacaran Ocean

Chao Li,[1]* Gordon D. Love,[1] Timothy W. Lyons,[1] David A. Fike,[2] Alex L. Sessions,[3] Xuelei Chu[4]

The Ediacaran Period (635 to 542 million years ago) was a time of fundamental environmental and evolutionary change, culminating in the first appearance of macroscopic animals. Here, we present a detailed spatial and temporal record of Ediacaran ocean chemistry for the Doushantuo Formation in the Nanhua Basin, South China. We find evidence for a metastable zone of euxinic (anoxic and sulfidic) waters impinging on the continental shelf and sandwiched within ferruginous [Fe(II)-enriched] deep waters. A stratified ocean with coeval oxic, sulfidic, and ferruginous zones, favored by overall low oceanic sulfate concentrations, was maintained dynamically throughout the Ediacaran Period. Our model reconciles seemingly conflicting geochemical redox conditions proposed previously for Ediacaran deep oceans and helps to explain the patchy temporal record of early metazoan fossils.

Numerous lines of geochemical and stable isotopic evidence have indicated that the Ediacaran (635 to 542 million years ago) ocean underwent a stepwise and protracted oxidation [e.g., (*1*–*4*)]. Some geochemical studies suggested that ocean basins were fully oxygenated by the late Ediacaran (*1*, *2*, *4*), yet others provided seemingly conflicting evidence for anoxic deep waters (*5*, *6*), with ferruginous conditions [Fe(II)-enriched] persisting into the Cambrian (*5*). Although a stratified ocean maintained through the Ediacaran Period (*7*) may help reconcile these seemingly conflicting views, the details remain unclear.

The Doushantuo Formation in the Nanhua Basin, South China, presents a unique opportunity to study Ediacaran ocean chemistry across spatial and temporal scales [e.g., (*8*)]. It is composed of a succession of both shallow- and deep-water siliciclastic, carbonate, and phosphatic sedimentary rocks deposited immediately after the last globally extensive Neoproterozoic glacial episode (*9*), widely known as the Marinoan glaciation. Zircon U-Pb ages indicate that the deposition of Doushantuo Formation lasted from ~635 to ~551 million years ago (*10*), spanning most of the Ediacaran Period.

To investigate the marine redox structure, we characterized the composition of sedimentary Fe mineral species and measured S isotope signatures for sulfides and sulfates (*11*) at four sections of Doushantuo Formation, which encompass the full range of sedimentary facies from continental shelf to slope to deep basin (fig. S1). We focused on quantifying the fractional abundance of Fe in several highly reactive mineral species (Fe_{HR}): pyrite (Fe_{Py}), Fe(III) oxides, magnetite, and carbonate minerals relative to total Fe (Fe_T) contents. High Fe_{HR}/Fe_T ratios indicate anoxic conditions (*12*). If anoxic, low associated Fe_{Py}/Fe_{HR} ratios indicate ferruginous bottom waters, whereas high Fe_{Py}/Fe_{HR} points to euxinic conditions, defined as having an anoxic and H_2S-containing water column (*5*, *12*). In most modern and ancient sediments deposited beneath anoxic bottom waters, Fe_{HR}/Fe_T exceeds 0.38, but this threshold value can be reduced to 0.15 [±0.10 (SD)] for thermally altered ancient sedimentary rocks (*13*) such as Doushantuo Formation because of conversion of Fe_{HR} to nonreactive iron during burial. For a euxinic water column, Fe_{Py}/Fe_{HR} in the underlying sediments usually exceeds 0.8 (*12*). Previous Fe speciation data obtained from Paleo- and Mesoproterozoic sedimentary rocks (*14*, *15*) revealed two distinct redox end members in marine basins characterized by either euxinic or ferruginous deep waters (fig. S2). In contrast, the iron speciation data from Doushantuo Formation are not confined to a single end member (Fig. 1A), suggesting nonuniform redox conditions for deep waters of Nanhua Basin.

The inner shelf Jiulongwan section records sedimentary deposition in the shallowest water

[1]Department of Earth Sciences, University of California, Riverside, CA 92521, USA. [2]Department of Earth and Planetary Sciences, Washington University, St. Louis, MO 63130, USA. [3]Department of Geological and Planetary Sciences, California Institute of Technology, Pasadena, CA 91125, USA. [4]State Key Laboratory of Lithospheric Evolution, Institute of Geology and Geophysics, Chinese Academy of Sciences, Beijing 100029, China.

*To whom correspondence should be addressed. E-mail: chaoli@ucr.edu

facies but well below wave base (*3*) and far from shore, along a broad continental shelf. The associated Fe data from this section plot in both the euxinic and ferruginous fields (Fig. 1A); late Ediacaran black shales from this section all plot in the euxinic zone (table S1). In contrast, samples from the Zhongling section, a deeper shelf margin setting, plot mainly in the ferruginous region, with only three samples having Fe_{Py}/Fe_{HR} ratios > 0.8 (Fig. 1A). The deepest water samples from the slope Minle and basinal Longe sections, which are all early Ediacaran black shales, contain very low levels of pyrite (thus low Fe_{Py}/Fe_{HR}) and yield Fe mineral parameters suggesting ferruginous bottom waters. Considering all the data, the paleoenvironmental trends suggest a co-occurrence of euxinic waters on the shelf with ferruginous deep water toward the center of the basin.

Carbonate lithologies dominate the shallow platform of Nanhua Basin, grading into shales in basinal settings (*16*, *17*), reflecting preferential precipitation of carbonates in shallower waters and enhanced hydrodynamic sorting of fine aluminosilicates into deeper waters. Accordingly, a stratigraphic decrease in carbonate content or, inversely, increasing Al content in samples (fig. S3) from the same site broadly reflects increasing water depth with rising sea level. Doushantuo samples exhibit two dominant trends when Fe_{Py}/Fe_{HR} ratios are viewed in light of Al concentration (Fig. 1B). Almost all inner shelf samples show an increase in Fe_{Py}/Fe_{HR} with increasing Al (path A in Fig. 1B), suggesting generally more sulfidic conditions with higher sea levels (greater distance from shore) but ferruginous conditions when sea level was lower. In contrast, most samples from distal sections show a reverse pattern (path B in Fig. 1B), with low Fe_{Py}/Fe_{HR} values found for samples with moderate-to-high Al content [>1 weight % (wt %)] regardless of organic content, suggesting a dominantly ferruginous and thus sulfate-limited deep-water setting. Taken together, these opposing trends can only be explained by a metastable mid–water-column sulfidic zone located between the inner shelf and the shelf margin nested within a ferruginous water mass (Fig. 2). The location and dimensions of this sulfidic zone would have fluctuated temporally. In most cases, euxinia is suggested independently by diagnostic Mo enrichments (fig. S4) above typical crustal values (*4*).

We did not observe direct evidence for oxic shallow waters in the sections that we sampled, although such conditions are expected in shallow settings given appreciable atmospheric O_2 in the Ediacaran atmosphere (*18*) and early benthic animal fossils at shallow sites (*19*–*22*). Therefore, it is likely that the sulfidic and ferruginous zones in the deep anoxic waters persisted beneath shallower oxic and ferruginous layers (Fig. 2).

It is difficult to envisage that a metastable sulfidic water mass could have coexisted with ferruginous deep water for 84 million years without mixing if seawater SO_4^{2-} concentration in Nanhua Basin was high. Net reduction in the surface S inventory may have limited the resupply of sulfate during the Neoproterozoic (*23*), particularly if reduced weathering during the Neoproterozoic glaciations suppressed the riverine flux (*24*). In combination with efficient sulfate removal from seawater through bacterial sulfate reduction and pyrite formation (*24*–*26*), enhanced by hydrothermal release of dissolved iron (*27*) during the glaciations and thereafter, this reduced delivery of sulfate reset Ediacaran ocean chemistry back to the ferruginous conditions (*5*) with extremely low SO_4^{2-} concentrations that have been prevalent in the Archean (*28*). Under such conditions, the continental sulfate supply was exhausted before reaching the deep basinal areas, resulting in a dynamically maintained lateral sulfate concentration gradient from shore to basin (Fig. 2, bottom inset) and, in turn, a metastable euxinic zone. Lack of sufficient sulfate to support extensive organic matter remineralization in distal marine settings is consistent with the large and long-stable pool of organic matter suggested for the deep Ediacaran ocean by the unusual carbon isotope systematics expressed in carbonate rocks and sedimentary organic matter of this age (*1*, *3*, *29*).

Several lines of evidence support the existence of a persistent sulfate concentration gradient in Nanhua Basin. First, larger ratios of organic C to pyrite S (C_{org}/S_{py}) in the distal sections (mean = 34, n = 49) compared with those of the inner shelf site (mean = 4, n = 42), similar to those found under modern low sulfate conditions (*30*), suggest lower sulfate concentrations in the distal regions (fig. S5). Second, an average offset of 30 per mil (‰) in the S isotope composition of pyrite ($\delta^{34}S_{py}$) was observed between most of the inner shelf and shelf margin sections (Fig. 3A), with ^{34}S-enriched pyrites formed in the deeper water settings. Furthermore, differences in S isotope ratios ($\Delta^{34}S$) between coeval carbonate-associated sulfate ($\delta^{34}S_{CAS}$) and $\delta^{34}S_{py}$ were on average ~10‰ lower for the shelf margin (~20‰) compared

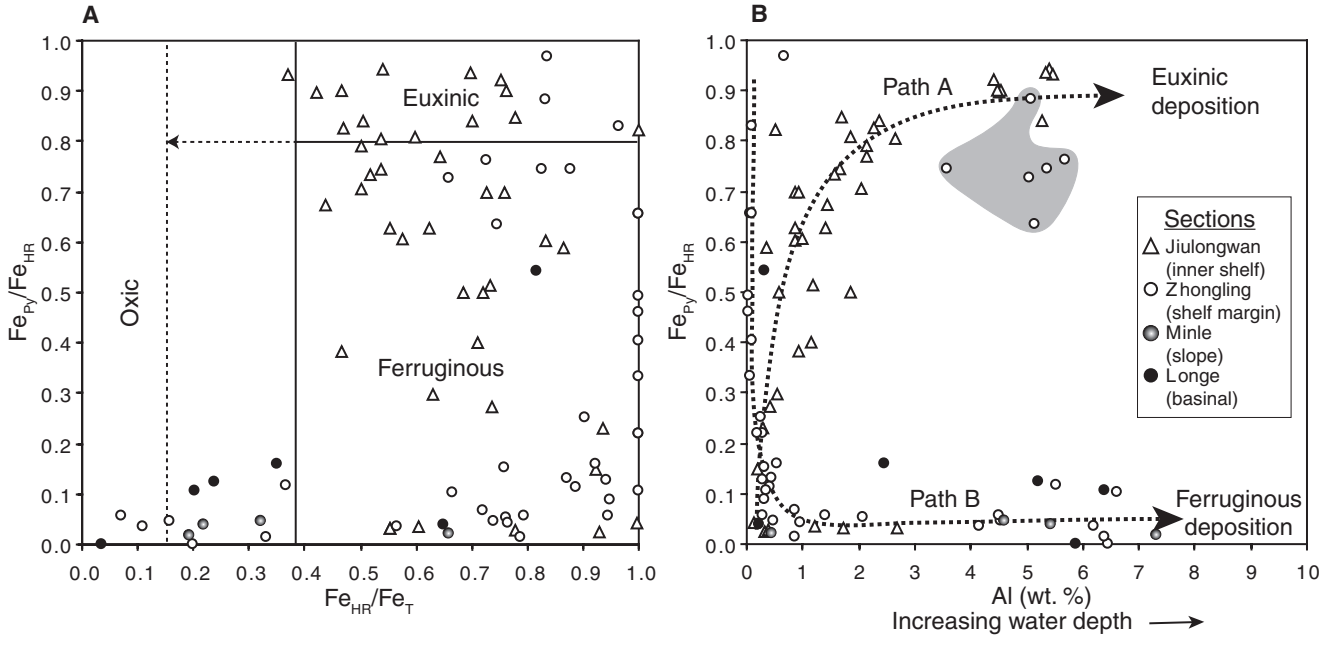

Fig. 1. (**A**) A crossplot of Fe_{Py}/Fe_{HR} versus Fe_{HR}/Fe_T shows a co-occurrence of euxinic with ferruginous conditions for deep waters of Nanhua Basin. Horizontal and vertical (solid for thermally immature and dashed for thermally mature rocks) lines indicate the boundaries for distinguishing euxinic from ferruginous and anoxic from oxic water columns. Dashed lines indicate the most appropriate boundary values for Doushantuo Formation. (**B**) Fe_{Py}/Fe_{HR} versus Al content shows two distinct redox profiles (path A and path B) that constrain the spatial location of the metastable sulfidic water mass to a region between the inner shelf and shelf margin. Samples in the shaded area were deposited in a stratigraphic interval during an early Ediacaran transgressive period and are outliers for path B.

with the inner shelf section (~30‰), suggesting lower SO_4^{2-} concentration availability along the shelf margin (Fig. 3B). Lastly, concentrations of carbonate-associated sulfate were consistently much lower for the shelf margin rocks compared with those from the inner shelf, with concentrations in the deeper sections frequently too low to permit isotopic analysis (table S1).

Modern seawater SO_4^{2-} concentration is ~28 mM, and the isotopic fractionation associated with bacterial sulfate reduction under such high sulfate availability is often large (up to 46‰). In contrast, limited fractionation occurs when sulfate concentration is low, particularly when it falls below a biological threshold of ~200 μM (*28*). These observations provide upper and lower limits for our estimates of SO_4^{2-} concentration in the Ediacaran Nanhua Basin, albeit within a broad range. The $\Delta^{34}S$ in the inner shelf Jiulongwan section increases abruptly from 1.5‰ in the basal cap carbonate to ~30‰ in the overlying ~40 m and thereafter, with a few samples having $\Delta^{34}S$ > 30‰ in the upper section (Fig. 3B). These trends are consistent with an increase of SO_4^{2-} concentration from <200 μM during post-Marinoan deglaciation to >200 μM thereafter and extending into the late Ediacaran. Although $\Delta^{34}S$ values from the shelf margin section are no more than 24‰, such fractionations are large enough to point to local sulfate levels > 200 μM during the late Ediacaran. The $\Delta^{34}S$ data do not provide a clear upper limit for late Ediacaran sulfate concentrations, but the isotopic and concentration gradients inferred from our study demand a sulfate level that was only a small fraction of the modern 28 mM.

Because the sulfidic zone could expand into previously oxygenated areas of the shelf during transgression and during pulses of high productivity, the generally patchy record of metazoans observed through the Ediacaran (*3*, *19*–*22*) might be explained by fluctuating oceanic redox conditions in and around the continental shelf. The finding of Ediacaran metazoan resting cysts, in the form of large ornamented acritarch fossils most prevalent in lower to middle Ediacaran strata from Doushantuo Formation (*19*) and from Australia and Russia (*22*), has previously been interpreted as an evolutionary response of early benthic metazoans to prolonged episodes of anoxia in shelf and platform bottom waters (*22*). Such a control is broadly consistent with our ocean redox model. For the inner shelf facies of Doushantuo Formation, available data highlight a broad correlation between sedimentary horizons containing the most diverse assemblage of acritarch fossils or animal embryos and intervals with the lowest pyrite contents (fig. S6), suggesting that the presence of hydrogen sulfide, rather than merely the absence of oxygen, hindered colonization of the shelf sea floor by early animals.

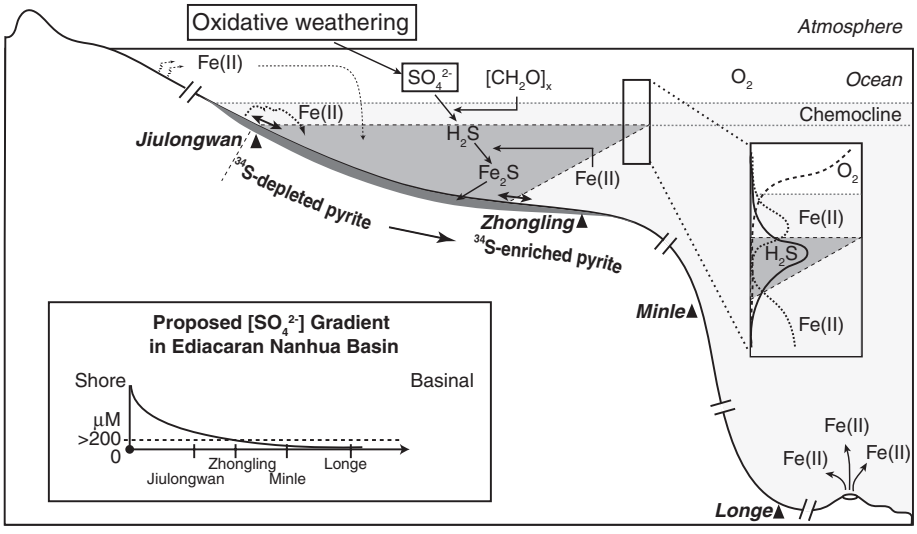

Fig. 2. Schematic representation of a stratified redox model for the Ediacaran Nanhua Basin. Most prevalent is a sulfidic water wedge, located at intermediate water depths within a ferruginous deep water mass and maintained by low riverine sulfate input and consumption of sulfate by bacterial sulfate reduction on the continental shelf. A lateral shore-to-basin sulfate concentration gradient (**bottom inset**) is assumed to be metastable.

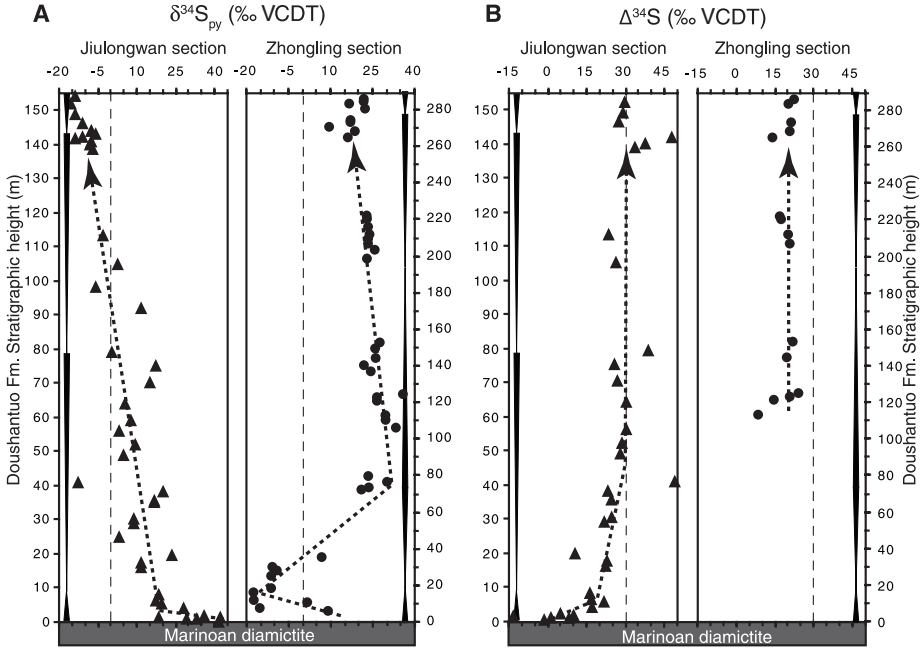

Fig. 3. Chemostratigraphic comparisons of (**A**) $\delta^{34}S_{py}$ and (**B**) $\Delta\delta^{34}S$ for inner shelf (Jiulongwan) and shelf margin (Zhongling) sections. The sections are correlated on the basis of alignment with published sequence stratigraphic data, and three similar transgressive-regressive sedimentary cycles can be identified (*3*, *16*). The lateral S-isotope gradient is also apparent when the sections are aligned by using carbonate C isotope stratigraphy (fig. S7). Values are reported relative to VCDT (Vienna Cañon Diablo Troilite) standard.

References and Notes

1. D. A. Fike, J. P. Grotzinger, L. M. Pratt, R. E. Summons, *Nature* **444**, 744 (2006).
2. D. E. Canfield, S. W. Poulton, G. M. Narbonne, *Science* **315**, 92 (2007); published online 7 December 2006 (10.1126/science.1135013).
3. K. A. McFadden *et al.*, *Proc. Natl. Acad. Sci. U.S.A.* **105**, 3197 (2008).
4. C. Scott *et al.*, *Nature* **452**, 456 (2008).
5. D. E. Canfield *et al.*, *Science* **321**, 949 (2008); published online 17 July 2008 (10.1126/science.1154499).
6. Y. Shen, T. Zhang, P. F. Hoffman, *Proc. Natl. Acad. Sci. U.S.A.* **105**, 7376 (2008).
7. G. A. Logan, J. M. Hayes, G. B. Hieshima, R. E. Summons, *Nature* **376**, 53 (1995).
8. G. Jiang, A. J. Kaufman, N. Christie-Blick, S. Zhang, H. Wu, *Earth Planet. Sci. Lett.* **261**, 303 (2007).
9. J. Wang, Z. X. Li, *Precambrian Res.* **122**, 141 (2003).
10. D. Condon *et al.*, *Science* **308**, 95 (2005); published online 24 February 2005 (10.1126/science.1107765).
11. See section of Materials and Methods in supporting material available on *Science* Online.
12. R. Raiswell, D. E. Canfield, *Am. J. Sci.* **298**, 219 (1998).
13. R. Raiswell *et al.*, *Am. J. Sci.* **308**, 105 (2008).
14. Y. Shen, A. H. Knoll, M. R. Walter, *Nature* **423**, 632 (2003).
15. S. W. Poulton, P. W. Fralick, D. E. Canfield, *Nature* **431**, 173 (2004).

16. M. Y. Zhu, J. M. Zhang, A. H. Yang, *Palaeogeogr. Palaeoclimatol. Palaeoecol.* **254**, 7 (2007).
17. E. Vernhet, C. Heubeck, M. Y. Zhu, J. M. Zhang, *Precambrian Res.* **148**, 32 (2006).
18. D. J. Des Marais, H. Strauss, R. E. Summons, J. M. Hayes, *Nature* **359**, 605 (1992).
19. L. Yin *et al.*, *Nature* **446**, 661 (2007).
20. S. Xiao, Y. Zhang, A. H. Knoll, *Nature* **391**, 553 (1998).
21. G. D. Love *et al.*, *Nature* **457**, 718 (2009).
22. P. A. Cohen, A. H. Knoll, R. B. Kodner, *Proc. Natl. Acad. Sci. U.S.A.* **106**, 6519 (2009), and references therein.
23. D. E. Canfield, *Am. J. Sci.* **304**, 839 (2004).
24. J. L. Kirschvink, in *The Proterozoic Biosphere: A Multidisciplinary Study*, J. W. Schopf, C. Klein, D. Des Maris, Eds. (Cambridge Univ. Press, Cambridge, 1992), pp. 51–52.
25. M. T. Hurtgen, M. A. Arthur, N. S. Suits, A. J. Kaufman, *Earth Planet. Sci. Lett.* **203**, 413 (2002).
26. P. Gorjan, J. J. Veevers, M. R. Walter, *Precambrian Res.* **100**, 151 (2000).
27. L. R. Kump, W. E. Seyfried Jr., *Earth Planet. Sci. Lett.* **235**, 654 (2005).
28. K. S. Habicht, M. Gade, B. Thamdrup, P. Berg, D. E. Canfield, *Science* **298**, 2372 (2002).
29. D. H. Rothman, J. M. Hayes, R. E. Summons, *Proc. Natl. Acad. Sci. U.S.A.* **100**, 8124 (2003).
30. R. A. Berner, R. Raiswell, *Geology* **12**, 365 (1984).
31. We are extremely grateful to R. Raiswell, S. Bates, W. Gilhooly, B. Gill, J. Owens, A. Khong, P. Marenco, N. Planavsky, C. Reinhard, M. Rohrssen, C. Scott, S. Severmann, J. Huang, L. Feng, H. Chang, and Q. Zhang for laboratory and field assistance and helpful discussions. The NSF Earth Sciences program (grant EAR-0720362 to G.D.L. and T.W.L. and grant EAR-0719493 to A.L.S.), National Science Foundation of China Fund (grant 40532012 to X.C.), the Chinese Academy of Sciences Fund (grant KZCX3-SW-141 to X.C.), the NASA Astrobiology Institute, and the Agouron Institute provided funding.

Supporting Online Material

www.sciencemag.org/cgi/content/full/science.1182369/DC1
Materials and Methods
Figs. S1 to S7
Table S1
References

23 September 2009; accepted 27 January 2010
Published online 11 February 2010;
10.1126/science.1182369
Include this information when citing this paper.

Mantle Flow Drives the Subsidence of Oceanic Plates

Claudia Adam[1,2]* and Valérie Vidal[3]

The subsidence of the sea floor is generally considered a consequence of its passive cooling and densifying since its formation at the ridge and is therefore regarded as a function of lithospheric age only. However, the lithosphere is defined as the thermal boundary layer of mantle convection, which should thus determine its structure. We examined the evolution of the lithosphere structure and depth along trajectories representative of the underlying mantle flow. We show that along these flow lines, the sea-floor depth varies as the square root of the distance from the ridge (as given by the boundary-layer equation) along the entire plate, without any flattening. Contrary to previous models, no additional heat supply is required at the base of the lithosphere.

At mid-oceanic ridges, hot material rises and then cools while driven away to subduction zones, forming the tectonic plates. The structure of the lithosphere, as the upper thermal boundary layer, is determined by conductive cooling after its formation at the ridge. The lithosphere thickens away from the mid-oceanic ridge and, as rock density increases by cooling, slowly sinks into the underlying mantle. Therefore, the sea-floor depth is regarded as a function of its age only and is studied along trajectories following an age gradient (referred to as "age trajectories"). Several models have been proposed to describe the thermal subsidence of the sea floor with age (*1*–*4*), but no consensus has been reached on the origin of the flattening observed at old ages (*5*). These thermal subsidence models do not directly consider the role of convection in the underlying mantle, which deforms with a velocity on the order of a few centimeters per year. In particular, their description of passive lithosphere cooling ignores any change in plate motion (in other words, in mantle convection).

[1]Institute for Research on Earth Evolution, Japan Agency for Marine-Earth Science and Technology, 2-15 Natsushima, Yokosuka, 237-0061, Japan. [2]Centro de Geofísica, Universidade de Évora, Rua Romão Ramalho 59, 7002-554 Évora, Portugal. [3]Laboratoire de Physique, Université de Lyon, Ecole Normale Supérieure de Lyon–CNRS, 46 Allée d'Italie, 69364 Lyon cedex 07, France.

*To whom correspondence should be addressed. E-mail: adam@uevora.pt

The first model that proposed to explain the variations of sea-floor depth with age—the half-space model (*6*)—considered the lithosphere as the cold upper boundary layer of a cooling mantle, where the depth varies with the square root of the distance from the ridge. By assuming a constant plate velocity, the sea-floor depth varies with the square root of the age of the lithosphere. However, subsequent studies found that the observed sea-floor depth at old ages [>70 million years ago (Ma)] was substantially shallower than the model prediction (*1*, *2*). These studies suggested that the flattening observed at old ages could be accounted for by a model in which the lithosphere is considered as a rigid, cooling conductive plate with a constant basal temperature (plate model) (*2*, *3*, *7*). However, if this constant temperature at the base of the plate is a simple and convenient way to introduce the additional heat supply necessary to explain sea-floor flattening at old ages, there is no physical reason why this should be true for the entire plate. Different physical processes have been proposed to explain the origin of this additional heat supply: small-scale convection (*8*–*11*), upwelling mantle plumes (*12*, *13*), or internal heating, including radiogenic heating as well as the heating from secular cooling (*11*, *14*). Nonetheless, we still do not know which of these physical processes is truly responsible for the observed flattening at old ages.

Previous global models also do not account for possible variations of ridge temperature and depth, either spatial or temporal. Systematic studies of sea-floor subsidence along the East Pacific Rise, for instance, show that the ridge depth varies from 2000 to 3200 m, and the associated subsidence rate from 50 to 450 m/Ma$^{1/2}$ (*15*–*19*). These variations imply spatial mantle temperature variations of about ±100°C (*16*–*18*). Others suggested that the possible change through time of plate motion and plate-driving forces (*20*) [in particular, pulsations in sea-floor spreading rates (*21*), and a higher mean mantle temperature during the Mesozoic (*22*)] could be responsible for higher ridge height and subsidence rate during this period. Estimates of a mantle ~50°C warmer during the Mesozoic, for example, could explain much of the observed flattening relative to a boundary-layer model (*22*).

Regardless of their differences, all previous models are based on the hypothesis that the thermal structure of the oceanic lithosphere is determined entirely by its age—that is, the time elapsed since its creation at the mid-oceanic ridge. However, because mantle convection and plate motion evolve over time, the new thermal conditions imposed on the base of the oceanic lithosphere also change, thus modifying its structure. This lithospheric structure will evolve to adapt to the new thermal conditions imposed at its base, along the entire plate. After a drastic change in the convective system, it will either thicken (or, alternately, become thinner) if the temperature at its base, defined by the new convective system, is cooler (or hotter) than it was previously. After a time long enough (several tens of million years), the lithosphere will tend toward the structure of the thermal boundary layer for the new underlying mantle flow, independently of its initial state.

To test that the structure of the oceanic lithosphere is determined by the underlying mantle convection, we analyzed more than 770 depth profiles, leading to a complete coverage of the Pacific plate (*23*). Several kinematic models have been tested to compute the trajectories representative of the present-day mantle convection (flow lines) (*23*). The Pacific plate is an ideal candidate to test our hypothesis for a number of reasons. First, the Pacific plate velocity has remained constant over the last 47 to 50 million years (My) (*24*), providing sufficient time for the lithosphere to